

Arresting Quantum Chaos Dynamically in Transmon Arrays

Rohit Mukherjee,* Haoyu Guo,* Keiran Lewellen, and Debanjan Chowdhury†
Department of Physics, Cornell University, Ithaca NY 14853.

Ergodic quantum many-body systems evolving under unitary time dynamics typically lose memory of their initial state via information scrambling. Here we consider a paradigmatic translationally invariant many-body Hamiltonian of interacting bosons — a Josephson junction array in the transmon regime — in the presence of a strong Floquet drive. Generically, such a time-dependent drive is expected to heat the system to an effectively infinite temperature, featureless state in the late-time limit. However, using numerical exact-diagonalization we find evidence of special ratios of the drive amplitude and frequency where the system develops *emergent* conservation laws, and *approximate* integrability. Remarkably, at these same set of points, the Lyapunov exponent associated with the semi-classical dynamics for the coupled many-body equations of motion drops by orders of magnitude, arresting the growth of chaos. We supplement our numerical results with an analytical Floquet-Magnus expansion that includes higher-order corrections, and capture the slow dynamics that controls decay away from exact freezing.

Contents

I. Introduction	1
II. Preliminaries: Model and Methods	2
A. Coupled Transmons	3
B. Semi-Classical Limit	3
C. Floquet Theory	4
III. Results from Exact Diagonalization	5
A. Square-Wave Drive	6
B. Oscillatory Drive	6
IV. Results in the Semi-Classical Limit	6
V. Floquet-Magnus Expansion	8
VI. Outlook	11
A. Analytical details of the Floquet-Magnus Expansion	12
1. General Expression for the Floquet Hamiltonian	12
2. Magnus Expansion of the Transmon Hamiltonian	12
B. Role of Hilbert-space Dimension and Initial State on Freezing	13
References	14

I. Introduction

The thermalization dynamics associated with closed quantum many-body systems evolving under their unitary dynamics has been at the center of attention over

the past few decades [1–4]. An intense scrutiny of non-integrable, translationally invariant interacting Hamiltonians, both in theory and experiment, has highlighted the role of the eigenstate thermalization hypothesis (ETH) in the approach to equilibrium. Thermalization proceeds through distinct stages, ranging from local relaxation to scrambling, and is intimately connected to the quantum chaotic nature of the many-body system. Exceptions to such equilibration can arise in strongly disordered problems that can possibly lead to many-body localization (MBL) [5–9], or in strongly constrained problems that host quantum “scar” states [10–12]. One of the appeals of arresting the onset of thermalization in many-body systems is their ability to preserve the memory associated with an initial state up to late times. However, the stability of MBL as a distinct phase of matter in the thermodynamic limit remains unclear [13–17], and the fraction of scar states in the many-body spectrum of many-body Hamiltonians is vanishingly small.

A special class of thermalization dynamics arises in the context of driven many-body systems, such as time-periodic Floquet Hamiltonians. In the absence of strong disorder leading to possible Floquet-MBL or time-crystalline ordered phases [18–21], such driven Hamiltonians thermalize to a completely featureless state with effectively “infinite-temperature” at asymptotically late times [22, 23]. However, under special circumstances, the heating can be slow with a long regime of a pre-thermal phase [24–27]. Thus, in generic quantum many-body Hamiltonians with or without a drive, it is difficult to arrest the growth of quantum chaos and prevent thermalization that eventually leads to a complete loss of the memory tied to the initial state.

In parallel developments, based on numerical exact diagonalization (ED) methods and some analytical perturbation theory, it has been suggested that spin models with a bounded local Hilbert space dimension subjected to a strong time-periodic Floquet drive display varying levels of “freezing” at a sequence of special ratios of the drive amplitude and drive frequency [28–40]. At these points, the system develops approximate emergent con-

* These authors contributed equally to this work

† debanjanchowdhury@cornell.edu

ervation laws. The degree to which the system freezes remains unclear, with some conjectures for spin-1/2 models suggesting an exact freezing [41]. Interestingly, the location of the above freezing-points coincide with the points at which the leading contribution in a Floquet-Magnus expansion vanish. However, there are a number of questions that remain. This includes (i) the role of the local Hilbert space dimension, including an unbounded spectrum, on freezing, (ii) the structure of the higher-order corrections, which controls both the exact location of the freezing point and the residual slow relaxation at freezing, and (iii) the nature of chaos, or lack thereof, at and near freezing. In an accompanying paper [42], some of us have addressed a subset of these questions definitively in an exactly solvable zero-dimensional model of chaotic quantum dots. Furthermore, we also identified a general criterion for freezing, which will be tested in the present manuscript, namely that whenever the commutator between the driving term and the non-integrable part of the static Hamiltonian has a quantized spectrum, the system is prone to display freezing.

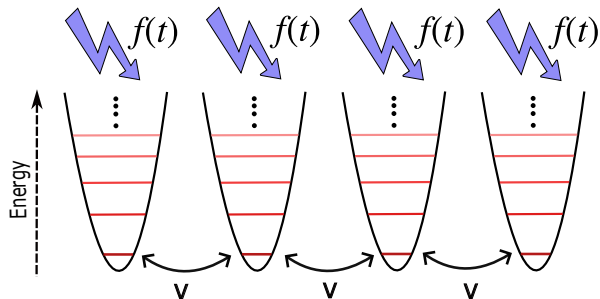


FIG. 1: Schematic representation of an array of transmons with an unbounded spectrum coupled via capacitive interactions. The external Floquet drive, $f(t)$, couples capacitively to each transmon.

In this manuscript, we address all of these fundamental questions regarding dynamical freezing using a multi-pronged approach. We focus on a paradigmatic model of enormous contemporary interest, namely an array of Josephson junctions (Fig. 1), which forms the fundamental building block of superconducting “transmon” based quantum computing [43, 44]. A single transmon setup consists of a Josephson junction and a shunting capacitance; the array is constructed out of capacitively coupled transmons. The transmon eigenspectrum is unbounded, but a few of the low lying eigenstates can be chosen to store quantum information. In the transmon regime, the Josephson energy (E_J) is much greater than the charging energy (E_C) with typical values in the range $E_J/E_C \sim 20 - 80$ [45]. Physically, the transmon array is a quantum version of coupled nonlinear pendula (i.e. oscillators) [46]. Based on a quantum-to-classical correspondence, it was pointed out that the transmon array shows strong signatures of chaos [46, 47], which can become a future impediment towards scaling up the arrays to tens of thousands of qubits. As the transmons are ex-

cited to higher energies, the nonlinearities become more pronounced and trigger a transition from integrable to chaotic motion. In this work we propose that dynamical freezing can be used effectively for suppressing chaos in a large array of transmons, and perhaps other related qubit architectures in the future.

In present day hardware, there are generally two ways by which the parasitic effects of chaos are minimized. The first strategy is to use tunable couplers that control the qubit-qubit interaction by changing the coupler frequency. In this way, qubits are decoupled when off-operation [48]. This approach is adapted by Google’s Sycamore device [49, 50]. A different strategy is to detune the oscillator frequency of neighboring qubits by varying their Josephson energy, which is used by IBM chips [51]. While the first approach stabilizes the system, the additional elements in the circuit add architectural complexity and may introduce new channels of decoherence. In the second approach, the intentional frequency detuning (“disorder”) effectively forces the bosonic quantum many-body system to become many-body localized, and thereby integrable. Whether this is a viable approach with increasing system volume is presently unclear. Regardless of the above protocol, finding new ways to dynamically protect the information stored in individual qubits in the NISQ era devices [52] is a desirable but challenging goal [53].

The remainder of this manuscript is organized as follows. In Sec. II, we introduce the model Hamiltonian of interest and describe the different technical tools that will be used to analyze it in the regime of a strong Floquet drive. These tools include numerical exact diagonalization, a solution for the associated semi-classical Hamiltonian’s equations of motion, and an analytical Floquet-Magnus expansion. In Sec. III we will discuss the results obtained using exact diagonalization and analyze a variety of diagnostics associated with freezing. We focus on the explicit computation of the semi-classical trajectories and the Lyapunov exponents in Sec. IV. In Sec. V, we extend the computations within a Floquet-Magnus expansion to include the higher-order corrections near freezing and compare against the numerical results. We end in Sec. VI with an outlook towards some open problems. The appendices A and B include a variety of additional technical details.

II. Preliminaries: Model and Methods

We introduce the transmon Hamiltonian of interest and discuss the different drive protocols in Sec. II A, followed by a description of the semi-classical analysis in Sec. II B. In Sec. II C, we review key elements of a Floquet-Magnus expansion, which will form the analytical basis for comparing against the numerical results.

A. Coupled Transmons

The model of interest to us is an array of coupled transmons [47] in the presence of an external time-periodic drive. The total Hamiltonian is composed of three different parts,

$$H(t) = \mathcal{H}_{\hat{n}}^0 + \mathcal{H}_{\hat{\varphi}}^0 + f(t)\mathcal{H}_{\hat{n}}^{\text{drive}}, \quad (1a)$$

$$\mathcal{H}_{\hat{n}}^0 = 4E_c \sum_i \hat{n}_i^2 + V \sum_{\langle i,j \rangle} \hat{n}_i \hat{n}_j, \quad (1b)$$

$$\mathcal{H}_{\hat{\varphi}}^0 = - \sum_i E_{J_i} \cos(\hat{\varphi}_i), \quad (1c)$$

$$\mathcal{H}_{\hat{n}}^{\text{drive}} = \sum_i \hat{n}_i, \quad (1d)$$

where \hat{n}_i is the Cooper pair number operator, $\hat{\varphi}_i$ is the superconducting phase at site i (which is compact and takes value in the range $(-\pi, \pi]$), E_c is the capacitive charging energy, E_{J_i} represent the Josephson energies of the individual transmons (in principle, drawn from some narrow normal distribution), and V is the coupling between nearest-neighbor transmons; see Fig. 1. Physically, E_J corresponds to the ability of Cooper pairs to tunnel across the junction. The canonically conjugate operators, \hat{n} , $\hat{\varphi}$ obey the usual commutation relation $[\hat{\varphi}_i, \hat{n}_j] = i\delta_{ij}$, and can be expressed as [54],

$$\hat{\varphi}_i = \left(\frac{2E_c}{E_{J_i}}\right)^{1/4} [a_i^\dagger + a_i], \quad \hat{n}_i = \frac{i}{2} \left(\frac{E_{J_i}}{2E_c}\right)^{1/4} [a_i^\dagger - a_i], \quad (2)$$

where a_i^\dagger , a_i represent bosonic creation and annihilation operators, respectively. Note that the spectrum and the associated local Hilbert space for the static Hamiltonian is unbounded from above, which *a priori* makes the fate of any freezing type phenomenology far from obvious. In particular, the nature of Fock-space (de-)localization, quantum interference, and approach to equilibration via chaos, can be distinctly different in the transmon model compared to spin-models. Interestingly, a Floquet drive-induced many-body localization has been analyzed in a one-dimensional weakly disordered bosonic Hamiltonian [55], where the drive effectively suppresses the static hopping amplitude [56] and pushes the system towards the MBL phase. In contrast, this work focuses on a translationally invariant Hamiltonian, where the static many-body system is fully ergodic and the emergent (approximate) integrability arises via a distinct mechanism.

For simplicity, we have ignored the offset charge(s) [57], $n_g(t)$, which are known to be a source of decoherence in charge qubits [58, 59]. In what follows and unless otherwise stated, we will assume a translationally invariant Hamiltonian with uniform Josephson energies, E_J ; we will briefly comment on the results including the role of randomness in these couplings at the end. We will restrict our attention to the usual transmon regime characterized by $E_J \gg E_c$ with an eye towards making connection to present day hardware, but the freezing phe-

nomenology is not solely restricted to this hierarchy of energy scales.

Now we turn our attention to the main ingredient, the Floquet drive, $f(t)$ with a period T , such that $f(t) = f(t+T)$; equivalently the drive frequency, $\omega = 2\pi/T$. For the sake of concreteness, we will focus on two types of drives (square wave and cosine wave, respectively) with an amplitude A in the remainder of this study:

$$\text{Case I: } f_{\text{I}}(t) = A \operatorname{sgn}[\sin(\omega t)], \quad (3a)$$

$$\text{Case II: } f_{\text{II}}(t) = A \cos(\omega t). \quad (3b)$$

Our focus in the remainder of this manuscript will be on the quantum dynamics, chaos and freezing (or lack thereof) for the model introduced in Eq. 1a due to the drive in Eq. 3a-3b as a function of A/ω . We will start by performing an ED analysis in Sec. III below. Given the unbounded local Hilbert-space, \mathcal{H}_D , we will analyze the eigenspectrum of $H(t)$ with a varying truncation scheme while expanding the $\cos(\dots)$ non-linearity in powers of $\hat{\varphi}$; see also Appendix B.

For the numerical results presented in the remainder of this manuscript, we will use the IBM parameters [60], $E_J = 12.58$ GHz, $E_c = 330$ MHz, $V = 50$ MHz. The transmon regime is defined by $E_J \gg E_c$, where the oscillator frequency for each transmon is given by $\nu_i = \sqrt{8E_J E_c} - E_c$ and is of the order of $\nu \sim 5$ GHz.

B. Semi-Classical Limit

The dynamics of the coupled transmons is amenable to a semi-classical analysis, where we replace the non-commuting operators $\hat{\varphi}$ and \hat{n} by classical real variables, and treating the commutator bracket as a Poisson bracket, $\{\varphi_i, n_j\} = \delta_{ij}$, respectively. Recall that in the absence of a Floquet drive, the semi-classical dynamics of transmon arrays has been analyzed, and the behavior is generically expected to be chaotic [46, 61] without substantial frequency detuning or tunable coupling [47]. Our goal will be to study how the Floquet drive in the absence of any other strategy helps arrest the growth of chaos, and protect the memory associated with generic initial states.

The Hamilton equations of motion for the coupled set of phase and number variables in Eq. 1a are given by,

$$\begin{aligned} \dot{\varphi}_i &= \{\varphi_i, \mathcal{H}\} = \frac{\partial \mathcal{H}}{\partial n_i} = 8E_c n_i + V \sum_{j \in \text{adj}_i} n_j + f(t) \quad (4a) \\ \dot{n}_i &= \{n_i, \mathcal{H}\} = -\frac{\partial \mathcal{H}}{\partial \varphi_i} = -E_{J_i} \sin \varphi_i, \quad (4b) \end{aligned}$$

where $\sum_{j \in \text{adj}_i}$ extends over the nearest neighbors of i . In the language of pendula the interaction between the transmons is a momentum-momentum interaction that is due to the capacitive coupling. In addition to obtaining the full dynamics associated with $\varphi_i(t)$, $n_i(t)$, we will

also diagnose chaos by computing the Lyapunov exponent [62]. Specifically, we focus on the maximal Lyapunov exponent (MLE), λ_L , which determines the rate at which trajectories that are initially “close” by diverge with time, $\delta\pi(t) \approx \delta\pi \exp(\lambda_L t)$. By contrasting the Lyapunov exponent for the static vs. driven transmon arrays, we will highlight in Sec. IV how dynamical freezing effectively arrests the growth of chaos at special values of A/ω .

C. Floquet Theory

Our time-dependent Hamiltonian $H(t) = H_0 + H_D(t)$ consists of two parts — the static piece, $H_0 \equiv \mathcal{H}_{\hat{n}}^0 + \mathcal{H}_{\hat{\varphi}}^0$, and the driven piece, $H_D(t) \equiv f(t)\mathcal{H}_{\hat{n}}^{\text{drive}}$. Due to the discrete time translational symmetry associated with the period $T \equiv 2\pi/\omega$, the solutions of the Schrödinger equation can be written as $|\psi_\alpha(t)\rangle = e^{-i\epsilon_\alpha t} |u_\alpha(t)\rangle$, with time-periodic Floquet wavefunction, $|u_\alpha(t+T)\rangle = |u_\alpha(t)\rangle$, and Floquet quasi-energy, $\epsilon_\alpha \in (-\omega/2, \omega/2]$, respectively. The Floquet-Schrödinger equation is written as [63, 64],

$$[H(t) - i\partial_t] |u_\alpha(t)\rangle = \epsilon_\alpha |u_\alpha(t)\rangle. \quad (5)$$

The Floquet eigenspectrum can be obtained by diagonalizing the effective Floquet Hamiltonian, H_{eff} , such that

$$\begin{aligned} U(T, 0) |u_\alpha(0)\rangle &= \exp[-iH_{\text{eff}}] |u_\alpha(0)\rangle \\ &= \exp(-i\epsilon_\alpha T) |u_\alpha(0)\rangle, \end{aligned} \quad (6)$$

where $U(t, t')$ is the usual time evolution operator $U(t, t') |\psi(t')\rangle = |\psi(t)\rangle$,

$$U(t, t') = \mathcal{T} \exp\left(-i \int_{t'}^t dt'' H(t'')\right), \quad (7)$$

and \mathcal{T} takes time-ordering into account. We are interested in the late time behavior of the system, and not on the detailed time dependence within individual periods. Hence, we will be primarily interested in the stroboscopic evolution of various observables which can be described by the effective Floquet Hamiltonian H_{eff} .

In the limit of both large driving amplitude and frequency, H_{eff} can be obtained from the modified Magnus expansion [33], which we review now. We consider moving into the co-moving frame of the driving term, via the unitary transform

$$W(t) = \exp(-i\theta(t)\mathcal{H}_{\hat{n}}^{\text{drive}}), \quad (8)$$

where $\theta(t) = \int_0^t dt' f(t')$ with the explicit form

$$\text{Case I: } \theta(t) = \frac{2\pi A}{\omega} [1/2 - \{|\omega t/(2\pi)\} - 1/2], \quad (9a)$$

$$\text{Case II: } \theta(t) = \frac{A}{\omega} \sin \omega t. \quad (9b)$$

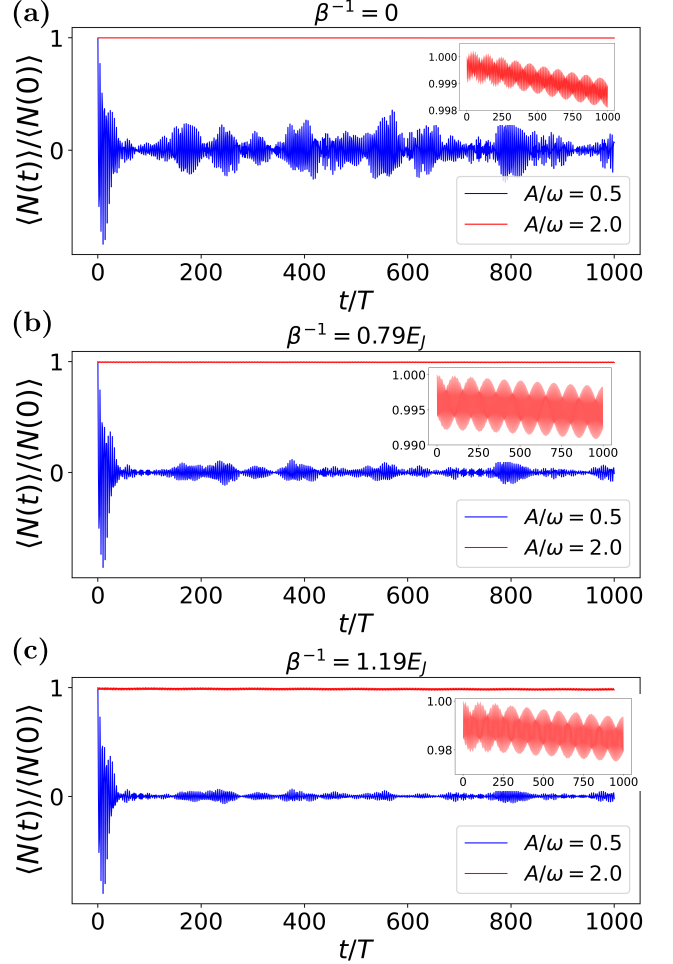


FIG. 2: Stroboscopic time evolution of normalized $\hat{N}(t)$ for different driving strengths for the square drive in Eq. 3a. The system size is $L = 8$, with an on-site Hilbert space dimension $\mathcal{H}_D = 3$. The drive frequency $\omega = 9.32$ GHz, and other parameters are as introduced in the main text. The initial state corresponds to the: (a) ground state, or thermal pure state with (b) $\beta^{-1} = 0.79E_J$, (c) $\beta^{-1} = 1.19E_J$, of $H(0)$. At freezing, there is a slow decay of the normalized $\langle \hat{N}(t) \rangle$ over time (inset).

Here $\{x\}$ means taking the decimal parts of x . The co-moving Hamiltonian is given by

$$\begin{aligned} \mathcal{H}_{\text{mov}}(t) &= W(t)^\dagger [H(t) - i\partial_t] W(t) \\ &= W(t)^\dagger (\mathcal{H}_{\hat{n}}^0 + \mathcal{H}_{\hat{\varphi}}^0) W(t), \end{aligned} \quad (10)$$

which is nominally independent of the large driving term $\mathcal{H}_{\hat{n}}^{\text{drive}}$. The co-moving Hamiltonian \mathcal{H}_{mov} can be evaluated using the Baker-Campbell-Hausdorff formula, and the result is:

$$\mathcal{H}_{\text{mov}}(t) = \mathcal{H}_{\hat{n}}^0[\hat{n}_i] + \mathcal{H}_{\hat{\varphi}}^0[\hat{\varphi}_i - \theta(t)]. \quad (11)$$

The Magnus expansion [33] states that the leading order Floquet effective Hamiltonian is given by the one-period

average of $\mathcal{H}_{\text{mov}}(t)$:

$$\mathcal{H}_{\text{eff}}^0 = \frac{1}{T} \int_0^T dt \mathcal{H}_{\text{mov}}(t). \quad (12)$$

For the model under consideration, we find

$$\mathcal{H}_{\text{eff}}^0 = \mathcal{H}_{\hat{n}_i}^0 - \sum_i \frac{\omega E_J}{\pi A} [\sin(\hat{\varphi}_i) + \sin(A\pi/\omega - \hat{\varphi}_i)] + \dots, \quad (13a)$$

$$\mathcal{H}_{\text{eff}}^0 = \mathcal{H}_{\hat{n}_i}^0 - E_J J_0 \left(\frac{A}{\omega} \right) \sum_i \cos(\hat{\varphi}_i) + \dots \quad (13b)$$

Here ... denote higher order corrections in $1/\omega$ which will be studied in further detail in Sec. V; see also Appendix A. Therefore, we find at a set of isolated points, the non-commuting φ -dependent terms vanish, and the effective Hamiltonian becomes seemingly integrable (at leading order):

$$\text{Case I: } \frac{A}{\omega} \approx 2n, \quad n \in \mathbb{Z}, \quad (14a)$$

$$\text{Case II: } \frac{A}{\omega} \approx \text{zeros of Bessel function } J_0. \quad (14b)$$

Given the structure of freezing and the form of the underlying drive Hamiltonian, we expect that the quantity $\hat{N} = (1/L) \sum_i \hat{n}_i$, or any operator that commutes with \hat{N} develops an emergent conservation law. The extent of thermalization can become extremely slow at the freezing points, in marked contrast to the rapid relaxation away from freezing.

III. Results from Exact Diagonalization

We begin by analyzing the emergent conservation law tied to \hat{N} from the ED computations. In this regard, the quantity of principle interest is the expectation value,

$$\langle \hat{N} \rangle = \frac{1}{L} \sum_i^L \langle \psi(t) | \hat{n}_i | \psi(t) \rangle, \quad (15)$$

starting from a specific initial state $|\psi(0)\rangle$, which yields the associated time evolved state, $|\psi(t)\rangle$. Freezing is identified by the asymptotic late-time behavior of this quantity, which is analyzed as a function of the parameter A/ω . Recall that without the drive, the Hamiltonian $H_0 \equiv \mathcal{H}_{\hat{n}_i}^0 + \mathcal{H}_{\hat{\varphi}}^0$ is known to be ergodic and chaotic [46], and since \hat{N} is not a conserved operator its expectation value is expected to relax rapidly. We also compute the time averaged (over Floquet cycles) quantity,

$$\mathcal{F} = \overline{\langle \hat{N}(t) \rangle} / \langle \hat{N}(0) \rangle, \quad (16)$$

at and away from freezing, which will help determine the shift of the freezing point due to higher order corrections.

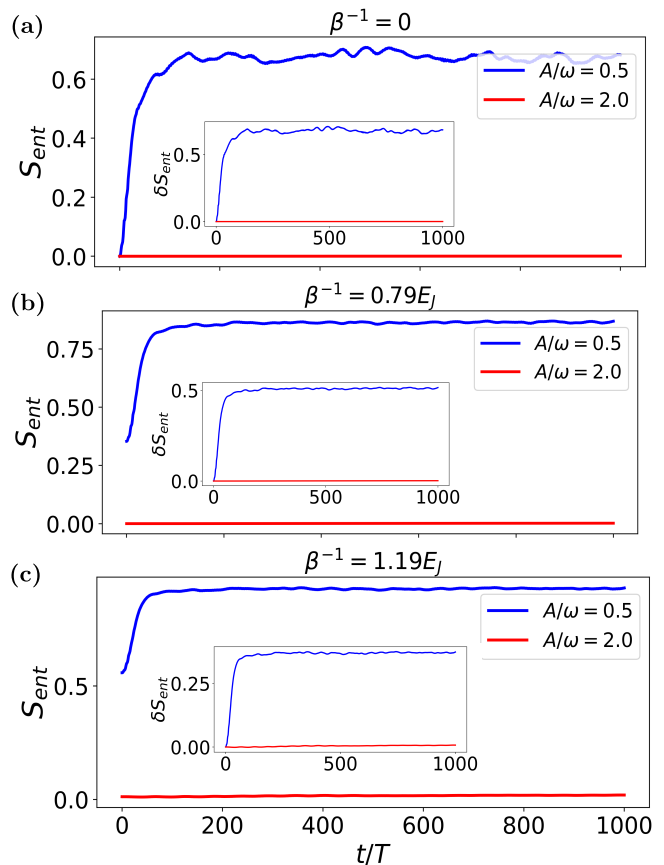


FIG. 3: Stroboscopic evolution of half-chain entanglement entropy at (red) and away from (blue) freezing for a square-wave drive for three different values of the initial temperature, β^{-1} . All of the system parameters are same as in Fig. 2. In the inset, we plot the relative change in entropy. The initial states are thermal pure states constructed out of $H(0)$, which includes the drive Hamiltonian.

We have performed the ED computations for a variety of system sizes, $L(= 6, 8)$, and on-site Hilbert space dimension, $\mathcal{H}_D(= 2, 3, 4)$. We initialize the computation in the time domain with different initial states, $|\psi(0)\rangle$, which are either eigenstates of $H(0)$ (which includes the drive term), or thermal superposition states constructed out of these, $\propto \sum_n e^{-\beta \epsilon_n} |n\rangle$. Unless otherwise stated, the default choice for the initial state is the ground state of $H(0)$. We notice that most eigenstates of $H(0)$, *except* the states in the middle of the spectrum, can be frozen at A/ω close to the prediction of the leading order Magnus expansion. For many-body states in the middle of the spectrum, the expectation values for $\langle \hat{n}_i \rangle$ become progressively smaller and the entanglement entropy saturates (see below) in a fashion that makes it numerically difficult to assess the extent of freezing.

We also analyze the entanglement entropy (EE) of the system, at and away from freezing, for a variety of initial states. The half-chain EE is defined as,

$$S_{\text{ent}} = -\text{Tr}[\rho_{\frac{1}{2}} \log \rho_{\frac{1}{2}}], \quad (17)$$

where $\rho_{\frac{1}{2}}$ is the density matrix of one half of the chain, computed by tracing out the other half. The entanglement dynamics between different parts of a system serves as a useful diagnostic for identifying the growth of quantum chaos [65]. A non-integrable Floquet system that thermalizes generically at late times, shows a saturating behavior for S_{ent} . The saturation value depends on the Hilbert space dimension, and is described by a volume law scaling [66]. However, when the system becomes dynamically frozen, the system develops approximate integrability and leads to extremely slow dynamics. This behavior should be evident in the overall suppression and slow growth of S_{ent} . Note that at the freezing point, due to Hilbert space fragmentation [67], the quantum state cannot access the full Hilbert space. Instead, it can only evolve under the invariant Krylov subspace. The dimension of this subspace is much smaller than the dimension of the Hilbert space, and this can lead to Rabi-type oscillations in the entanglement entropy. Finally, we note that the exact nature of the residual dynamics in the frozen state can, in principle, be dependent on the choice of the initial state, which will be analyzed below.

In order to highlight the salient features of the freezing phenomenology that emerges under the square vs. cosine-wave drives, we discuss these separately below in the following two subsections.

A. Square-Wave Drive

In Fig. 2, we plot the stroboscopic time evolution for the operator \hat{N} (defined in Eq. 15), normalized by its initial value. We start either with the ground state of the total Hamiltonian at time $t = 0$, or a thermal superposition of the eigenstates of $H(0)$, defined as $|\Psi(0)\rangle = \sum_n \exp(-\beta\epsilon_n) |\psi_n\rangle$. When the amplitude of the drive is away from freezing, the system loses memory of the initial state rapidly. On the other hand, at the freezing point, there is an approximate emergent conservation law associated with \hat{N} , and the system retains its memory up to late times. However, we emphasize that this emergent conservation is only approximate, and in Sec. V we calculate the corrections to freezing within a Magnus expansion, which are small in $\mathcal{O}(1/\omega)$. Moreover, these corrections can also result in a shift of the location for freezing. Interestingly, the corrections can depend on the choice of initial states, which therefore also affects the robustness of the associated freezing phenomenology.

In Fig. 3 we show the stroboscopic time evolution of the growth of half chain many-body quantum entanglement entropy (S_{ent}) for different initial states. Away from freezing, S_{ent} grows rapidly and saturates to its equilibrated value. At freezing, the system becomes approximately integrable, and the growth of EE becomes slow while its saturation value depends on the Hilbert space dimension of the fragmented sector.

B. Oscillatory Drive

For the cosine drive, let us first present results for the numerically time-averaged quantity introduced in Eq. 16 in Fig. 4. We find that the choice of initial state has a strong effect on the location of freezing, i.e. \mathcal{F} peaks at a value of A/ω that is renormalized away from the value predicted by the zeroth-order Magnus expansion in Eq. 14b. We will revisit this renormalization from the point of view of the higher order corrections in $\mathcal{O}(1/\omega)$ in Sec. V.

In Fig. 5, we revisit the stroboscopic time evolution for $\hat{N}(t)$ at the numerically determined renormalized freezing points (Fig. 4). For $|\psi(0)\rangle$, we choose both the ground state and an excited eigenstate of $H(0)$; \hat{N} becomes approximately conserved at the renormalized freezing points. The slow time decay associated with the emergent conservation in Fig. 5(c) is controlled by the higher order corrections in the Magnus expansion.

Finally, in Fig. 6 we show the stroboscopic evolution of the half-chain entanglement entropy. At the renormalized freezing points (indicated by red curves), there is a noticeable slow increase in the entanglement entropy compared to the square-wave drive. The difference stems primarily from the structure of higher-order corrections in a Magnus expansion; while the first-order correction for the square-wave drive is zero, it is non-zero for the oscillatory drive. However, away from freezing (represented by the blue curves), the system rapidly thermalizes, and the difference from the frozen curve is striking.

IV. Results in the Semi-Classical Limit

The coupled semi-classical equations of motion in Eq. 4a-4b for φ_i and n_i can be solved using a Tsitouras 5/4 Runge-Kutta method [68], starting from a specific initial state. One of our main goals in this section will be to analyze the chaotic properties associated with the resulting trajectories. Consider two trajectories in phase space with an infinitesimal initial separation $\delta\pi_0$ at time $t = 0$, and let $\delta\pi(t)$ be the resulting separation at a later time t . The maximal Lyapunov exponent is defined as [69]

$$\lambda_L = \lim_{t \rightarrow \infty} \lim_{|\delta\pi_0| \rightarrow 0} \frac{1}{t} \log \left(\frac{|\delta\pi(t)|}{|\delta\pi_0|} \right). \quad (18)$$

In order to pick a starting state that has a close correspondence with realistic “computational states” in the quantum problem, we adapt the strategy highlighted in Ref. [46]. First we calculate the eigenenergies, E_m , for a single static quantum transmon. The energies of the computational states are given by E_0 , E_1 for the $|0\rangle$, $|1\rangle$ state, respectively. We then initialize the transmons in the semiclassical limit as 0 or 1 by initializing their phase space coordinates as $(n, \varphi) = (0, \varphi_m)$, where $-E_J \cos \varphi_m = E_m$ for $m = 0, 1$. In this fashion we can

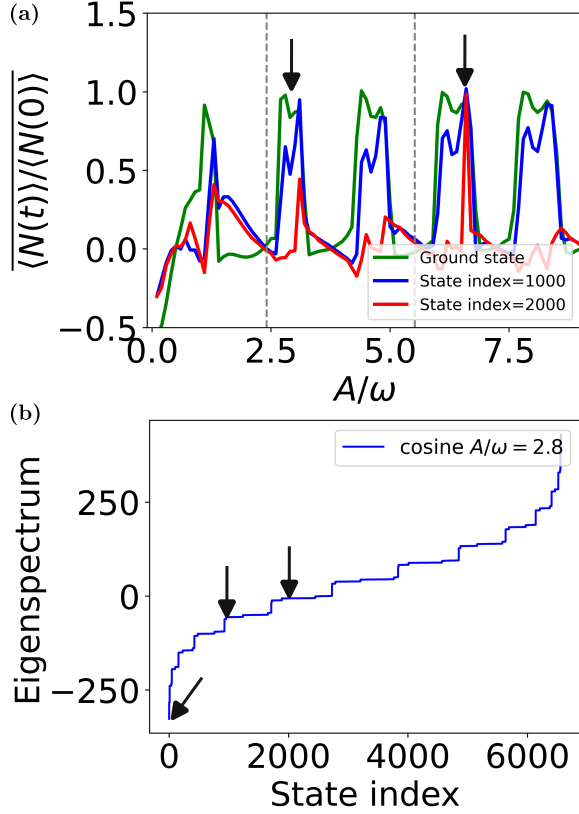


FIG. 4: (a) Time-averaged \mathcal{F} (averaged over 100 Floquet cycles) as a function of A/ω for the cosine drive. We choose $|\psi(0)\rangle$ from the eigenspectrum of $H(0)$, with their “state-index” sorted by energy eigenvalue. Primary freezing points, indicated by arrows, shift from the zeroth-order prediction of freezing point in Eq. 14b (dashed lines). The shift can be explained based on the higher order corrections in the Magnus expansion, discussed in Sec. V. (b) The eigenspectrum of the Hamiltonian $H(0)$ is plotted along with their corresponding Fock state indices. The states chosen to calculate $\langle \hat{N}(t) \rangle$ are indicated with arrows.

initialize semi-classical states as 101010..., that mimic the corresponding quantum state. The Lyapunov spectrum is computed using the “H2 method” [70, 71], and implemented in Julia [72].

We begin first by discussing the results for the square-wave drive in Eq. 3a. In Fig. 7(a) we plot the MLE as a function of the drive amplitude, A , for a fixed drive frequency, ω . Remarkably, whenever A/ω approaches the special points in Eq. 14a, λ_L is suppressed by several orders in magnitude compared to the value in the static case (shown by dashed line). Relatedly, to highlight the correspondence between the quantum and classical results, we evaluate $\langle \hat{N}(t) \rangle$ (normalized by its initial value) from the ED data, and λ_L using the semiclassical equations as a function of the ratio of the drive to transmon frequencies, respectively. The results are shown in Fig. 7(b) at a fixed value of $A/\omega = 2$, which corresponds to one of the freezing points. Clearly, both sets of re-

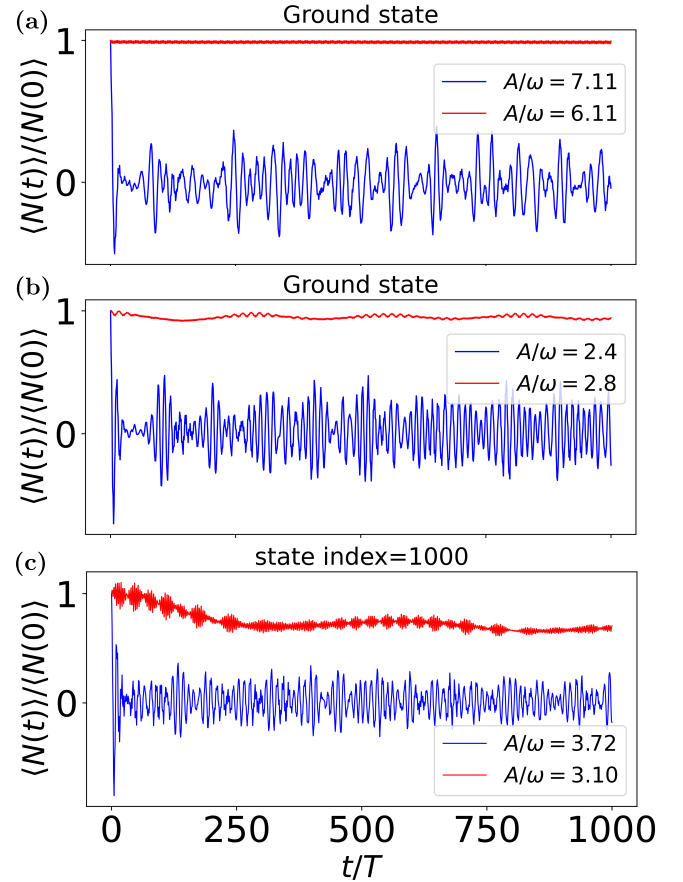


FIG. 5: Stroboscopic time evolution of normalized $\hat{N}(t)$ for the cosine drive given by Eq.(3b). The system size is $L = 8$, with an on-site Hilbert space dimension $\mathcal{H}_D = 3$. The drive frequency $\omega = 9.32$ GHz, and other parameters are as introduced in the main text. The initial state are chosen from the eigenstates of $H(0)$. The renormalized freezing points are obtained from Fig. 4.

sults suggest that freezing requires a lower cutoff on the drive frequency, set roughly by the individual transmon frequency. We have also noticed that for a given value of ω , freezing requires the amplitude to be larger than a critical value.

To help visualize how the trajectories for $\{\varphi, n\}$ evolve with varying A/ω for the square-wave drive, we generate phase-space portraits for two transmons (picked at random) from the total system consisting of $L = 8$ transmons. When the system is away from freezing, and starting from an initial state 1010..., the phase-space fills up uniformly over time and displays ergodic behavior as shown in Fig. 8(a). Specifically, n displays strong fluctuations over time starting from its initial value. In contrast, at freezing the individual transmons exhibit strong deviations away from any ergodic behavior (Fig. 8(b)), leading to a highly constrained set of trajectories in phase-space showing minimal fluctuations of n .

Finally, turning over to the cosine drive, Fig. 9 shows

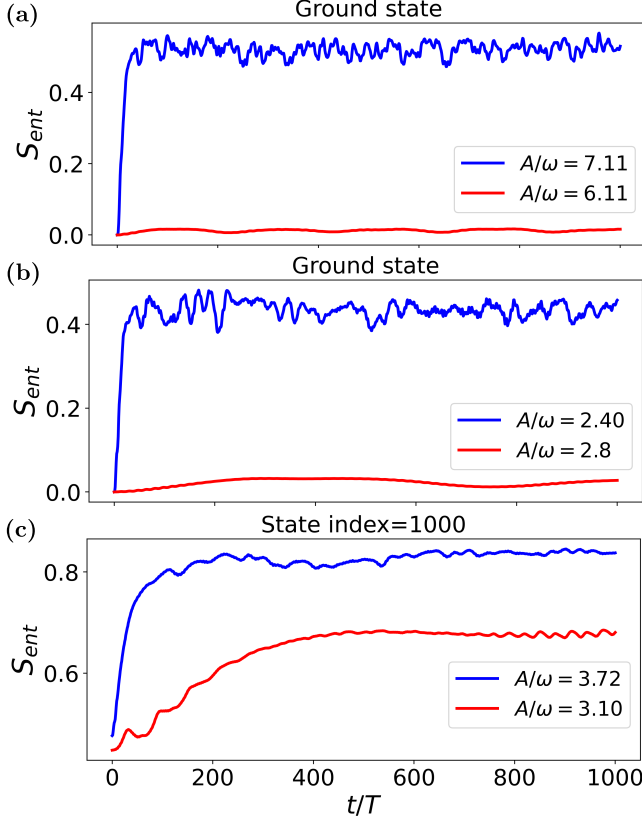


FIG. 6: Stroboscopic evolution of half-chain entanglement entropy at (red), and away from (blue) freezing for a cosine wave drive for the parameters in Fig. 5 for different initial states, $|\psi(0)\rangle$.

a plot of λ_L as a function of A/ω for an $L = 8$ transmon array. Once again, we find that λ_L drops significantly at freezing compared to the static Hamiltonian. However, the location of the freezing points is not determined by the zeroth-order Magnus expansion, as was noted in the ED analysis as well, highlighting the significant role played by the higher order corrections.

V. Floquet-Magnus Expansion

In this section, we extend the Floquet-Magnus expansion for the transmon Hamiltonian beyond the leading order discussed previously in Eq. 13a-13b. In particular, we use the expansion to compute the renormalized freezing point. As will become clear later, it will be useful to consider the drive amplitude to vary across different sites. Thus we modify the drive term as,

$$\mathcal{H}_{\hat{n}}^{\text{drive}} = \sum_i f_i(t) \hat{n}_i, \quad (19)$$

where $f_i(t) = A_i \cos(\omega t)$, or $A_i \text{sgn}[\sin(\omega t)]$. The co-moving Hamiltonian therefore becomes

$$\mathcal{H}_{\text{mov}}(t) = \mathcal{H}_{\hat{n}}^0[\hat{n}_i] + \mathcal{H}_{\hat{\varphi}}^0[\hat{\varphi}_i - \theta_i(t)], \quad (20)$$

where the θ_i is expressed as an integral over the f_i 's as in Eq. 8, but is position-dependent now.

The first few terms in the Magnus expansion of the Floquet Hamiltonian in terms of the co-moving Hamiltonian Eq. 10 are given by

$$\mathcal{H}_{\text{eff}}^0 = \frac{1}{T} \int dt \mathcal{H}_{\text{mov}}(t), \quad (21a)$$

$$\mathcal{H}_{\text{eff}}^1 = \frac{1}{2iT} \int_0^T dt_1 \int_0^{t_1} dt_2 [\mathcal{H}_{\text{mov}}(t_1), \mathcal{H}_{\text{mov}}(t_2)], \quad (21b)$$

$$\mathcal{H}_{\text{eff}}^2 = \frac{-1}{6T} \int_0^T dt_1 \int_0^{t_1} dt_2 \int_0^{t_2} dt_3 ([\mathcal{H}_{\text{mov}}(t_1), [\mathcal{H}_{\text{mov}}(t_2), \mathcal{H}_{\text{mov}}(t_3)]] + (t_1 \leftrightarrow t_3)). \quad (21c)$$

The integrals can be evaluated analytically (see Appendix A), and we only summarize the results below. The zeroth-order term is,

$$\mathcal{H}_{\text{eff}}^0 = \mathcal{H}_{\hat{n}}^0 - \frac{E_J}{2} \sum_k \left(F_{0,k}^* e^{i\hat{\varphi}_k} + F_{0,k} e^{-i\hat{\varphi}_k} \right), \quad (22)$$

where $F_{m,k}$ is the Fourier coefficient of $e^{i\theta_k(t)}$:

$$e^{i\theta_k(t)} = \sum_m F_{m,k} e^{im\omega t}. \quad (23)$$

The explicit form of $F_{m,k}$ is

$$\text{Case I: } F_{m,k} = -\frac{iA_k\omega \left(-1 + (-1)^m e^{\frac{i\pi A_k}{\omega}} \right)}{\pi(A_k^2 - m^2\omega^2)} \quad (24a)$$

$$\text{Case II: } F_{m,k} = J_m \left(\frac{A_k}{\omega} \right). \quad (24b)$$

The first-order result is

$$\mathcal{H}_{\text{eff}}^1 = \frac{E_J}{2\omega} \sum_k \left[B_k \Delta_k \mathcal{H}_{\hat{n}}^0 e^{-i\hat{\varphi}_k} + \text{h.c.} \right], \quad (25)$$

where Δ_k is the finite difference at site k :

$$\Delta_k \mathcal{H}_{\hat{n}}^0[\hat{n}_1, \dots, \hat{n}_L] = \mathcal{H}_{\hat{n}}^0[\dots, (\hat{n}_k+1), \dots] - \mathcal{H}_{\hat{n}}^0[\dots, \hat{n}_k, \dots]. \quad (26)$$

For the $\mathcal{H}_{\hat{n}}^0$ given in Eq.(1b), the explicit form is given by,

$$\Delta_k \mathcal{H}_{\hat{n}}^0 = 4E_c(2\hat{n}_k + 1) + V \sum_{j \in \text{adj}_k} \hat{n}_j, \quad (27)$$

where j runs over the neighbors of site k .

The parameter B_k is

$$B_k = \sum_{m \neq 0} \frac{F_{m,k}}{m} = \begin{cases} 0, & \text{Case I;} \\ \frac{\pi}{2} \mathbf{H}_0 \left(\frac{A_k}{\omega} \right), & \text{Case II} \end{cases} \quad (28)$$

where the sum ranges over all non-zero integers m and \mathbf{H}_0 is the Struve function. Note that the first case sums to zero as $F_{m,k}/m$ is an odd function of m .

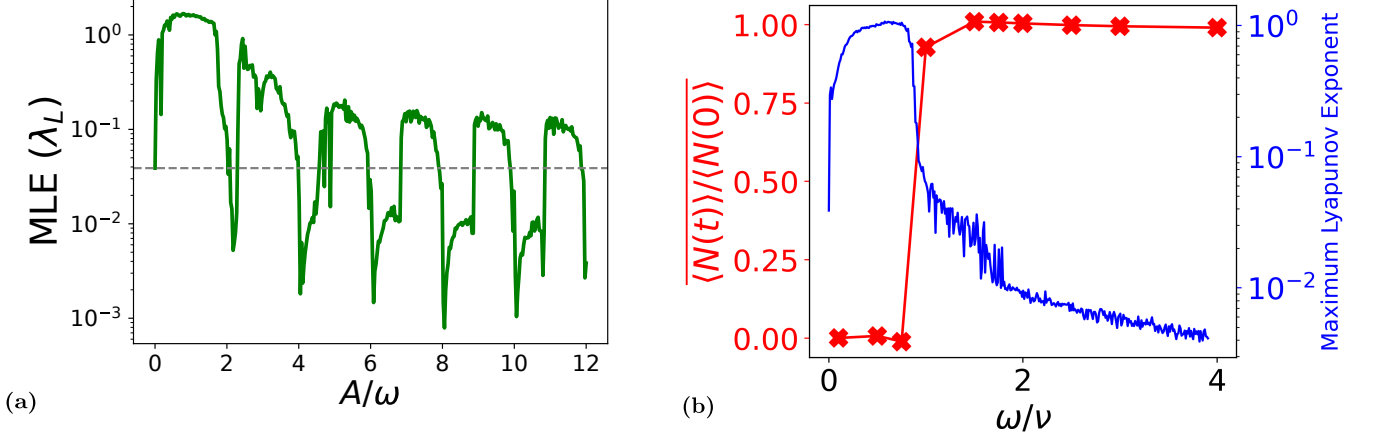


FIG. 7: (a) The maximum Lyapunov exponent (MLE), λ_L , as a function of A/ω for a fixed drive frequency ($\omega = 15$ GHz) with the square-wave drive, initialized in the 1010... state. The strong suppression of λ_L coincides with the location of freezing points in Eq. 14a. Dashed horizontal line shows λ_L for the static hamiltonian. (b) Correspondence between quantum and classical dynamics as a function of the ratio of drive frequency to transmon frequency at freezing with $A/\omega = 2$ kept fixed. The quantum expectation $\langle \hat{N}(t) \rangle$ is computed by time-averaging over 100 Floquet cycles in the ground state of $H(0)$. For both plots $L = 8$, $E_c = 12.58$ GHz, $E_J = 330$ MHz, and $V = 50$ MHz.

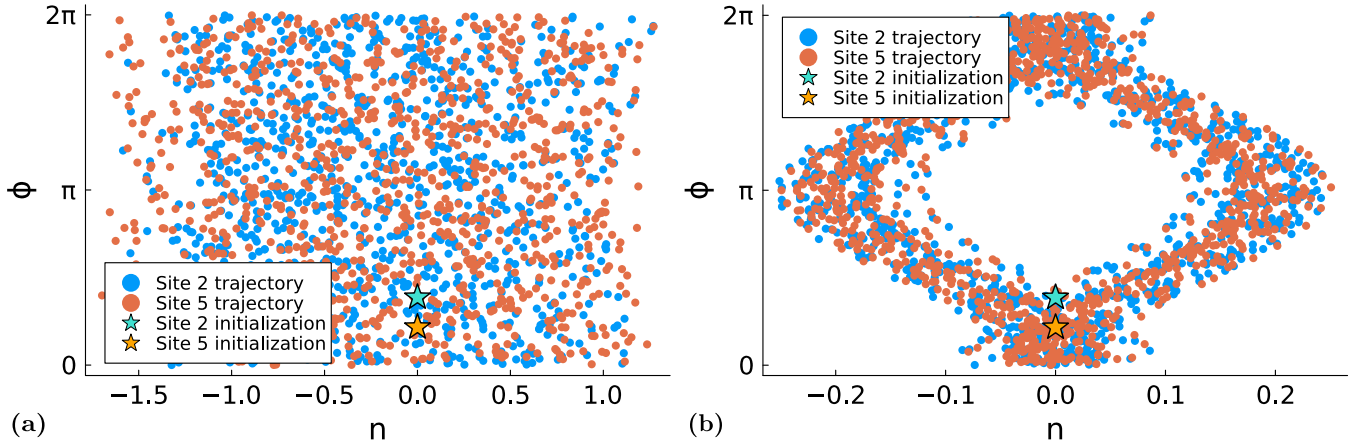


FIG. 8: Phase-space trajectories for two transmons (site 2 and 5, respectively) for an array with $L = 8$ transmons, for initial state 1010... and a square-wave drive with $\omega = 15$ GHz over 250 cycles. The values of the drive amplitude are (a) $A = 110$ GHz, and (b) $A = 120.36$ GHz (corresponding to $A/\omega = 8$), respectively.

Finally, the second-order result is the sum of three terms $\mathcal{H}_{\text{eff}}^2 = H_A^2 + H_B^2 + H_C^2$, where

$$H_A^2 = \frac{E_J^2}{8\omega^2} \sum_{kl} [B_k^* B_l^* e^{i\hat{\varphi}_k + i\hat{\varphi}_l} \Delta_k \Delta_l + B_l B_k^* e^{i\hat{\varphi}_k} \Delta_k \Delta_l \mathcal{H}_n^0 e^{-i\hat{\varphi}_l} + \text{h.c.}], \quad (29a)$$

$$H_B^2 = \frac{E_J^2}{4\omega^2} \sum_{kl} [C_k^* F_{0,l}^* e^{i\hat{\varphi}_k + i\hat{\varphi}_l} \Delta_k \Delta_l - C_k F_{0,l}^* e^{i\hat{\varphi}_k} \Delta_k \Delta_l \mathcal{H}_n^0 e^{-i\hat{\varphi}_l} + \text{h.c.}], \quad (29b)$$

$$H_C^2 = \frac{E_J}{2\omega^2} \sum_k [C_k^* e^{i\hat{\varphi}_k} (\Delta_k \mathcal{H}_n^0)^2 + \text{h.c.}]. \quad (29c)$$

The parameter C_k is

$$C_k = \sum_{m \neq 0} \frac{F_{m,k}}{m^2}. \quad (30)$$

Since $\Delta_k \Delta_l \mathcal{H}_n^0$ is only non-zero when k, l coincide, or are nearest neighbors, the second order corrections are still local Hamiltonians.

These results indicate that the Floquet-Magnus expansion is essentially a $1/\omega$ expansion, where the A/ω dependence of freezing enters via the magnitude of the coefficients of this expansion. Therefore, the expansion is expected to perform well in the high frequency limit.

Next, we consider the first-order renormalizations of

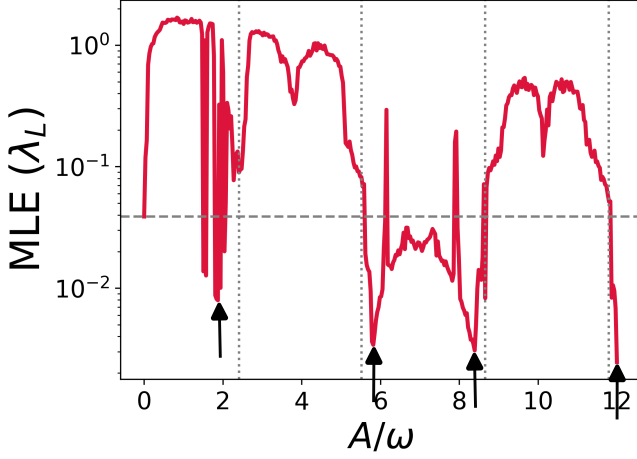


FIG. 9: The maximum Lyapunov exponent as a function of A/ω for the cosine drive. The system with $L = 8$ transmons is initialized in an 1010... state with a drive frequency $\omega = 15$ GHz. The freezing points are indicated by arrows. The horizontal dashed line indicates λ_L for the static Hamiltonian. The vertical dotted lines indicate the freezing points associated with the zeroth-order term in Eq. 14b.

the freezing point, which is especially relevant for the cosine drive in Eq. 3b. We write the Floquet Hamiltonian as $\mathcal{H}_{\text{eff}} = \mathcal{H}_{\hat{n}}^0 + U$, where

$$U = -\frac{E_J}{2} \sum_k \left[e^{-i\hat{\varphi}_k} \left(F_{0,k} - \frac{B_k}{\omega} \bar{\Delta}_k \mathcal{H}_{\hat{n}}^0 \right) + e^{i\hat{\varphi}_k} \left(F_{0,k}^* - \frac{B_k^*}{\omega} \Delta_k \mathcal{H}_{\hat{n}}^0 \right) \right]. \quad (31)$$

Notice that due to the non-commutativity between $\hat{\varphi}$ and \hat{n} , in the first line the forward difference Δ_k has been shifted to the backward difference $\bar{\Delta}_k$ when $e^{-i\hat{\varphi}_k}$ is commuted to the left:

$$\bar{\Delta}_k \mathcal{H}_{\hat{n}}^0[\hat{n}_1, \dots, \hat{n}_L] = \mathcal{H}_{\hat{n}}^0[\dots, \hat{n}_k, \dots] - \mathcal{H}_{\hat{n}}^0[\dots, \hat{n}_k - 1, \dots]. \quad (32)$$

We consider a particular initial state $|n\rangle$ which is the eigenstate of $\mathcal{H}_{\hat{n}}^0$ and labelled by n_i : $\mathcal{H}_{\hat{n}}^0 |n\rangle = E_n |n\rangle$, $\hat{n}_i |n\rangle = n_i |n\rangle$. To improve the freezing for state $|n\rangle$, we demand that the norm of $U |n\rangle$ should be minimized, which is achieved at

$$F_{0,k} = \frac{B_k}{2\omega} (\Delta_k E_n + \bar{\Delta}_k E_n), \quad (33)$$

where we have replaced $\mathcal{H}_{\hat{n}}^0$ by its eigenvalue E_n . Substituting the explicit expressions for the cosine drive (Eqs.(24), (27), (28)), we obtain

$$J_0 \left(\frac{A_k}{\omega} \right) = \frac{\pi}{2\omega} \mathbf{H}_0 \left(\frac{A_k}{\omega} \right) \left(8E_c n_k + V \sum_{j \in \text{adj}_k} n_j \right). \quad (34)$$

Eqs.(33) and (34) is the main result of this section, which indicates the first-order correction of the freezing point in

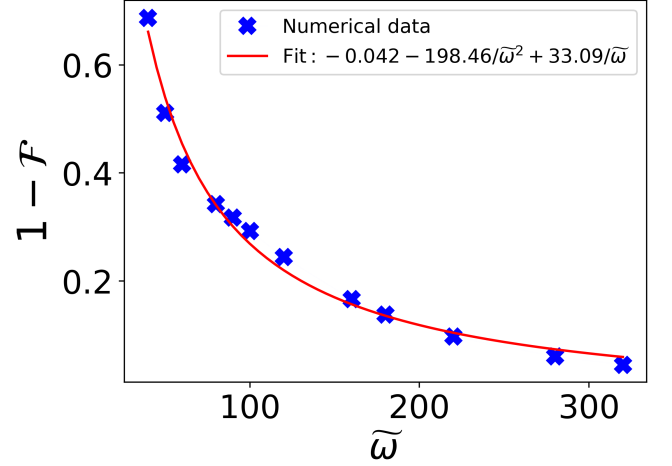


FIG. 10: The time-averaged observable, \mathcal{F} (Eq. 16), as a function of ω rescaled by the individual transmon frequency, ν . We choose $|\psi(0)\rangle$ as the ground state of $H(0)$ and fix $A/\omega = 2.4048$ at the first freezing point within the zeroth-order Magnus expansion. The scaling is predominantly proportional to $1/\omega$ (Eq. 25).

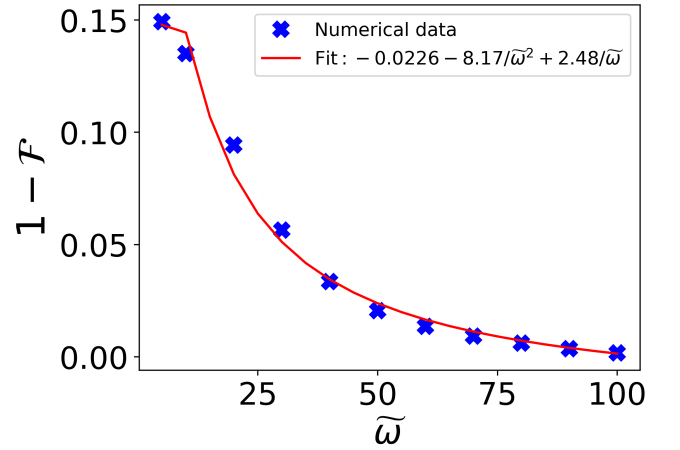


FIG. 11: \mathcal{F} as in Fig. 10, but at a value of A/ω which is set at the renormalized freezing point (taking into account the zeroth and first-order corrections). The parameters are the same as in Fig.10.

terms of the amplitude-frequency ratio A_k/ω . Notably, the right hand side of Eq. (34) is proportional to n_i . Thus, the magnitude of renormalization a state experiences from the zeroth order freezing value increases with increasing n_i .

We notice, however, that satisfying Eq. (33) does not completely eliminate the first-order corrections. At the first-order corrected freezing point (33), there is still a residual action of U on $|n\rangle$:

$$U |n\rangle = -2E_J E_c \sum_k \frac{B_k}{2\omega} \left[e^{-i\hat{\varphi}_k} - e^{i\hat{\varphi}_k} \right] |n\rangle. \quad (35)$$

This term arises exactly due to the non-commutativity

between $\Delta_k \mathcal{H}_n^0 = 4E_c(2\hat{n}_k + 1)$ and $e^{i\hat{\varphi}_k}$, which is the manifestation of uncertainty principle in the context of dynamical-freezing. We also note that the first-order renormalization depends on the initial state $|n\rangle$ and can be spatially inhomogeneous. In Figs. 10 and 11, we test our numerical results with the theoretical prediction of the freezing under cosine drive. We compared the decay rate of $\langle N(t) \rangle$ for A/ω at the zeroth-order freezing point and the first-order freezing point and performed a scaling analysis in ω . In both cases the decay rate primarily scales as $1/\omega$. We observe that the decay rate of $\langle N(t) \rangle$ is reduced at the first-order freezing point, in the sense that the coefficient of $1/\omega$ becomes smaller (but not vanishing). These behaviors agree with the theoretical prediction that the decay rate scales as $1/\omega$.

Next, we discuss the second-order corrections and focus on the square-wave drive Eq. 3a. Since $B_k = 0$ (see Eq. 28), the first-order correction vanishes. Among the second-order corrections, $H_A^2 = 0$ due to $B_k = 0$, $H_B^2 \sim 1/\omega^4$ due to $F_0 \sim 1/\omega^2$ and we therefore only need to consider H_C^2 . We note that because H_C^2 , similar to H_{eff}^0 , depends on $\hat{\varphi}$ only through single-site operators, it can be partially cancelled by adjusting A_k/ω . The computation of the renormalized freezing point proceeds similarly to the first-order case, with the result

$$F_{0,k} = \frac{C_k}{2\omega^2} [(\Delta_k E_n)^2 + (\bar{\Delta}_k E_n)^2]. \quad (36)$$

Substituting the parameters for the square-wave drive, the explicit equation for $\alpha_k = A_k/\omega$ for the renormalized freezing point is

$$\alpha_k^2 (e^{i\pi\alpha_k} - 1) = -\frac{(\Delta_k E_n)^2 + (\bar{\Delta}_k E_n)^2}{12\omega^2} \times [-6 - 6i\pi\alpha_k + 2\pi^2\alpha_k^2 + e^{i\pi\alpha_k}(6 + \pi^2\alpha_k^2)], \quad (37)$$

where

$$\Delta_k E_n = 4E_c(2n_k + 1) + V \sum_{j \in \text{adj}_k} n_j, \quad (38)$$

$$\bar{\Delta}_k E_n = 4E_c(2n_k - 1) + V \sum_{j \in \text{adj}_k} n_j. \quad (39)$$

Again, this does not completely cancel the second order correction due to non-commutativity, and we therefore expect the residual non-conservation rate to scales as $1/\omega^2$ for the system under square-wave drive.

We have performed ED computations including disordered couplings, E_J , drawn from a random distribution with a finite variance. For a small variance, the phenomenon of freezing persists. However, given our observation of the site-dependent corrections in the higher-order Magnus expansion, an increasing strength of disorder can affect the location of freezing. In the asymptotic sense, for any given strength of disorder, a strong enough drive frequency can be used to reinstate the freezing phenomenology in principle. However, we leave a detailed study of this for future work.

VI. Outlook

In this work, we have analyzed the phenomenon of dynamical freezing using a variety of complementary perspectives for a paradigmatic many-body system of coupled Josephson junctions. Freezing is demonstrated in an interacting translationally invariant system, and can be understood within an effective Floquet-Magnus high-frequency expansion. One of our most interesting observations is the semiclassical limit of dynamical freezing, where the solutions for the coupled Hamilton's equations of motion show a dramatic reduction of their chaotic properties at the frozen points. However, it is also clear that freezing is not exact, and we have been able to address both the renormalization of the freezing point and the residual slow dynamics due to the higher-order corrections within the same Floquet-Magnus expansion. Importantly, the structure of this expansion is dependent on the drive, making some drive protocols more resilient to the emergent conservation laws compared to others (e.g. square-wave vs. cosine-wave drive). Given our refined understanding of the structure of these corrections, it will be an interesting future exercise to consider more complex Floquet drive protocols that can diminish their effects.

Clearly, one practical application of this protocol will be to adapt it in a fashion where one is able to protect encoded information up to late times. In the current transmon-based setting, the key impediment towards this is due to the noisy offset charge [73, 74], which has been ignored for simplicity in our analysis. At the freezing point, where the Hamiltonian effectively becomes \mathcal{H}_n^0 , the spatio-temporal dependence of the offset charge can play a significant role in the decoherence. Finding alternative routes to mitigate this effect in a realistic superconducting device based architecture remains an exciting open direction.

Acknowledgments

We thank S.D. Börner, A. Das, V. Fatemi, B. Kobrin, Y. Lensky, R. Moessner, E. Rosenberg, P. Roushan, S. Roy, V. Smelyanskiy, C. Tahan, G. Vidal and B. Ware for a number of useful discussions leading up to this work. RM thanks M. Bukov and S. Bandyopadhyay for many useful suggestions regarding QuSpin PYTHON package [75, 76], and thanks S.D. Börner for providing the Julia code dynamical.jl [72] for solving the semiclassical equations for the transmon arrays. RM is supported by a Fulbright-Nehru Grant No. 2877/FNDR/2023-2024 sponsored by the Bureau of Educational and Cultural Affairs of the United States Department of State. HG is supported by a Wilkins postdoctoral fellowship at Cornell University. DC is supported in part by a New Frontier Grant awarded by the College of Arts and Sciences at Cornell University and by a Sloan research fellowship from the Alfred P. Sloan foundation.

A. Analytical details of the Floquet-Magnus Expansion

In this appendix, we provide additional details regarding the Floquet-Magnus expansion.

1. General Expression for the Floquet Hamiltonian

Continuing the discussion in the main text, we work in the co-moving frame of the drive Hamiltonian, where the time-evolution unitary is given by

$$U_I(t) = \mathcal{T} \exp \left(-i \int_0^t dt' \mathcal{H}_{\text{mov}}(t') \right), \quad (\text{A.1})$$

where \mathcal{T} denotes time ordering. $U_I(t)$ satisfies the Schrödinger equation in the interaction picture

$$i \partial_t U_I(t) = \mathcal{H}_{\text{mov}}(t) U_I(t). \quad (\text{A.2})$$

We can write $U_I(t) = \exp[\Omega(t)]$, where the Floquet Hamiltonian will be identified with $\mathcal{H}_{\text{eff}} = i\Omega(T)/T$. We can rewrite the derivative of $\partial_t U_I$ using the identity

$$\begin{aligned} \partial_t e^{\Omega(t)} &= \int_0^1 d\lambda e^{\lambda\Omega(t)} \partial_t \Omega(t) e^{(1-\lambda)\Omega(t)} \\ &= h(\text{ad}_{\Omega(t)}) \partial_t \Omega e^{\Omega(t)}, \end{aligned} \quad (\text{A.3})$$

where $h(x) = (e^x - 1)/x$ and $\text{ad}_X Y = [X, Y]$. Combining this with Eq. A.2, we obtain,

$$\partial_t \Omega(t) = -ih(\text{ad}_{\Omega(t)}) \mathcal{H}_{\text{mov}}(t). \quad (\text{A.4})$$

This equation can be integrated iteratively in powers of \mathcal{H}_{mov} with boundary condition $\Omega(0) = 0$, and we obtain the first few terms in the Magnus-Floquet expansion for \mathcal{H}_{eff} :

$$\mathcal{H}_{\text{eff}}^0 = \frac{1}{T} \int_0^T dt \mathcal{H}_{\text{mov}}(t), \quad (\text{A.5})$$

$$\mathcal{H}_{\text{eff}}^1 = \frac{1}{2iT} \int_0^T dt_1 \int_0^{t_1} dt_2 [\mathcal{H}_{\text{mov}}(t_1), \mathcal{H}_{\text{mov}}(t_2)], \quad (\text{A.6})$$

$$\begin{aligned} \mathcal{H}_{\text{eff}}^2 &= \frac{-1}{6T} \int_0^T dt_1 \int_0^{t_1} dt_2 \int_0^{t_2} dt_3 \\ &([\mathcal{H}_{\text{mov}}(t_1), [\mathcal{H}_{\text{mov}}(t_2), \mathcal{H}_{\text{mov}}(t_3)]] + (t_1 \leftrightarrow t_3)). \end{aligned} \quad (\text{A.7})$$

2. Magnus Expansion of the Transmon Hamiltonian

In this section we explicitly evaluate Eqs. A.5-A.7 for the transmon Hamiltonian. The co-moving Hamiltonian is given by

$$\mathcal{H}_{\text{mov}}(t) = \mathcal{H}_{\hat{n}}^0 - E_J \sum_k \cos(\hat{\varphi}_k - \theta_k(t)), \quad (\text{A.8})$$

where

$$\begin{aligned} \text{Case I: } \theta(t) &= \frac{2\pi A_k}{\omega} [1/2 - \{\omega t/(2\pi)\} - 1/2] \quad (\text{A.9a}) \\ \text{Case II: } \theta(t) &= \frac{A_k}{\omega} \sin \omega t. \end{aligned} \quad (\text{A.9b})$$

Here we have allowed the driving amplitude A_k to vary across lattice sites.

To evaluate the integrals in Eq. A.5-A.7, it is most convenient to decompose \mathcal{H}_{mov} in terms of Fourier components

$$\mathcal{H}_{\text{mov}}(t) = \sum_m h_m e^{im\omega t}, \quad (\text{A.10})$$

where

$$h_0 = \mathcal{H}_{\hat{n}}^0 - E_J \sum_k \frac{F_{0,k} e^{-i\hat{\varphi}_k} + F_{-0,k}^* e^{i\hat{\varphi}_k}}{2}, \quad (\text{A.11})$$

$$h_{m \neq 0} = -E_J \sum_k \frac{F_{m,k} e^{-i\hat{\varphi}_k} + F_{-m,k}^* e^{i\hat{\varphi}_k}}{2}, \quad (\text{A.12})$$

and $F_{m,k}$ is the Fourier coefficient of $e^{i\theta_k(t)}$:

$$e^{i\theta_k(t)} = \sum_m e^{im\omega t} F_{m,k}. \quad (\text{A.13})$$

The explicit expression for $F_{m,k}$ is given in Eq. 24 in the main text.

We proceed to compute the terms up to second order in the Floquet Hamiltonian. The zeroth-order result is simply

$$\mathcal{H}_{\text{eff}}^0 = h_0. \quad (\text{A.14})$$

The first-order Floquet Hamiltonian is

$$\mathcal{H}_{\text{eff}}^1 = \sum_{m,n} I_{mn}^{(1)} [h_m, h_n] = \sum_{m \neq 0} \left(I_{m0}^{(1)} - I_{0m}^{(1)} \right) [h_m, h_0], \quad (\text{A.15})$$

where in the second equality we have utilized that $[h_m, h_n] = 0$ for $m, n \neq 0$. The coefficient $I_{mn}^{(1)}$ is given by the integral

$$I_{mn}^{(1)} = \frac{1}{2iT} \int_0^T dt_1 \int_0^{t_1} dt_2 \exp(i\omega(mt_1 + nt_2)), \quad (\text{A.16})$$

and we obtain $I_{m0}^{(1)} = -I_{0m}^{(1)} = -1/(2m\omega)$. The last piece is to compute the commutator $[h_m, h_0]$, which can be readily done using the identity

$$[e^{i\hat{\varphi}_k}, G(\hat{n}_k)] = -e^{i\hat{\varphi}_k} \Delta_k G(\hat{n}_k), \quad (\text{A.17})$$

$$[e^{-i\hat{\varphi}_k}, G(\hat{n}_k)] = \Delta_k G(\hat{n}_k) e^{-i\hat{\varphi}_k}, \quad (\text{A.18})$$

where G is an arbitrary function of \hat{n}_k . Here $\Delta_k G(\hat{n}_k) = G(\hat{n}_k + 1) - G(\hat{n}_k)$ is the forward difference. We therefore arrive at the result

$$\mathcal{H}_{\text{eff}}^1 = \frac{E_J}{2\omega} \sum_k \left[B_k \Delta_k \mathcal{H}_{\hat{n}}^0 e^{-i\hat{\varphi}_k} + \text{h.c.} \right], \quad (\text{A.19})$$

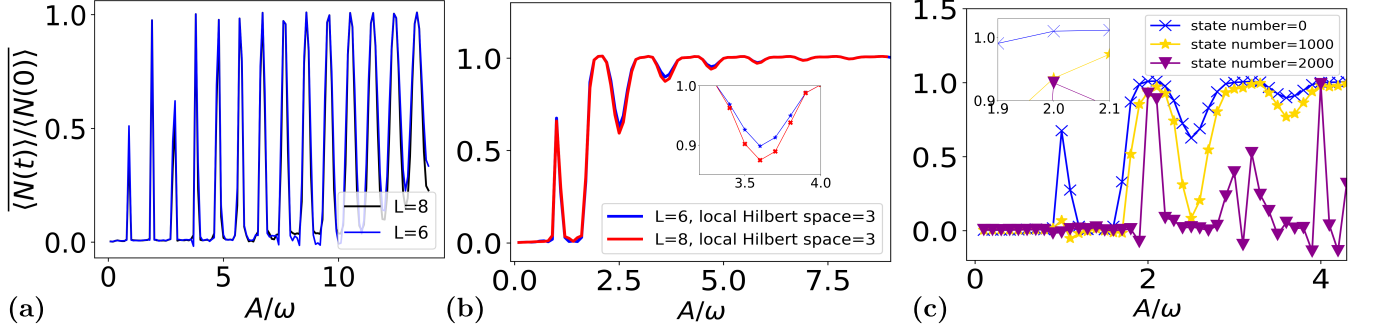


FIG. 12: (a) \mathcal{F} (Eq. 16) averaged over 100 Floquet cycles as a function of $\alpha = A/\omega$ for two different system sizes ($L = 6, 8$) and onsite Hilbert space ($\mathcal{H}_D = 2$), with $|\psi(0)\rangle$ chosen as ground state of $H(0)$. In addition to the sharp peaks at *even* integer α , peaks at *odd* integers are also seen. (b) Same as in (a), but with $\mathcal{H}_D = 3$. With increasing α , \mathcal{F} flattens out since \mathcal{H}_φ^0 weakens compared to $\mathcal{H}_\varphi^0 + f(t)\mathcal{H}_\varphi^{\text{drive}}$. (c) For $L = 8$ transmons and $\mathcal{H}_D = 3$, variation of \mathcal{F} for different $|\psi(0)\rangle$, drawn from the eigenspectrum of $H(0)$ in Fig. 13. All other parameters are as in Fig. 2.

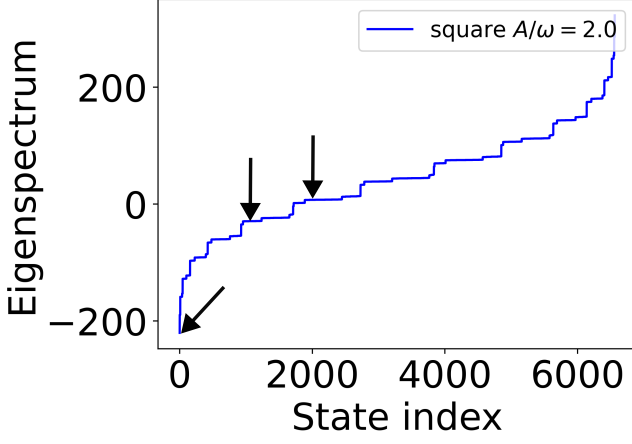


FIG. 13: The eigenspectrum of $H(0)$ for the square-wave drive, plotted with the corresponding Fock state indices. The eigenstates marked by arrows are used as $|\psi(0)\rangle$ to calculate the observables in Eq. 16 and Fig. 12.

where

$$B_k = \sum_{m \neq 0} \frac{F_{m,k}}{m}. \quad (\text{A.20})$$

Continuing on to the second order correction, the expression for the Floquet Hamiltonian is

$$\mathcal{H}_{\text{eff}}^2 = \sum_{mnk} (I_{mnk}^{(2)} + I_{knm}^{(2)}) [h_m, [h_n, h_k]], \quad (\text{A.21})$$

where

$$I_{mnk}^{(2)} = \frac{-1}{6T} \int_0^T dt_1 \int_0^{t_1} dt_2 \int_0^{t_2} dt_3 e^{i\Omega(mt_1 + nt_2 + kt_3)}. \quad (\text{A.22})$$

To have a nonzero commutator, we need at least $n = 0$

or $k = 0$,

$$\mathcal{H}_{\text{eff}}^2 = \sum_{mn} [h_m, [h_n, h_0]] \left(I_{mn0}^{(2)} + I_{0nm}^{(2)} - I_{m0n}^{(2)} - I_{n0m}^{(2)} \right). \quad (\text{A.23})$$

Therefore $n \neq 0$, and the rest can be decomposed into three parts:

$$H_A^2 = \sum_{m \neq 0, n \neq 0} [h_m, [h_n, h_0]] \left(I_{mn0}^{(2)} + I_{0nm}^{(2)} - I_{m0n}^{(2)} - I_{n0m}^{(2)} \right), \quad (\text{A.24a})$$

$$H_B^2 = \sum_{n \neq 0} [h_0 - \mathcal{H}_\varphi^0, [h_n, h_0]] \left(2I_{0n0}^{(2)} - I_{00n}^{(2)} - I_{n00}^{(2)} \right), \quad (\text{A.24b})$$

$$H_C^2 = \sum_{n \neq 0} [\mathcal{H}_\varphi^0, [h_n, h_0]] \left(2I_{0n0}^{(2)} - I_{00n}^{(2)} - I_{n00}^{(2)} \right). \quad (\text{A.24c})$$

The coefficients in the parenthesis above can be calculated and we obtain

$$\left(I_{mn0}^{(2)} + I_{0nm}^{(2)} - I_{m0n}^{(2)} - I_{n0m}^{(2)} \right)_S = \frac{1}{2mn\omega^2}, \quad (m, n \neq 0), \quad (\text{A.25a})$$

$$\left(2I_{0n0}^{(2)} - I_{00n}^{(2)} - I_{n00}^{(2)} \right) = \frac{1}{n^2\omega^2}, \quad (n \neq 0). \quad (\text{A.25b})$$

In Eq. A.25a, we have symmetrized the result with respect to $m \leftrightarrow n$ (indicated by the subscript S), because m, n can be exchanged in Eq. A.24a due to $[h_m, h_n] = 0$. The final step is to compute the commutators, and we obtain Eqs. (29) in the main text.

B. Role of Hilbert-space Dimension and Initial State on Freezing

In this appendix, we comment on the effect of increasing local Hilbert-space dimension (\mathcal{H}_D) and the choice of initial state (e.g. picked from the eigenspectrum) on

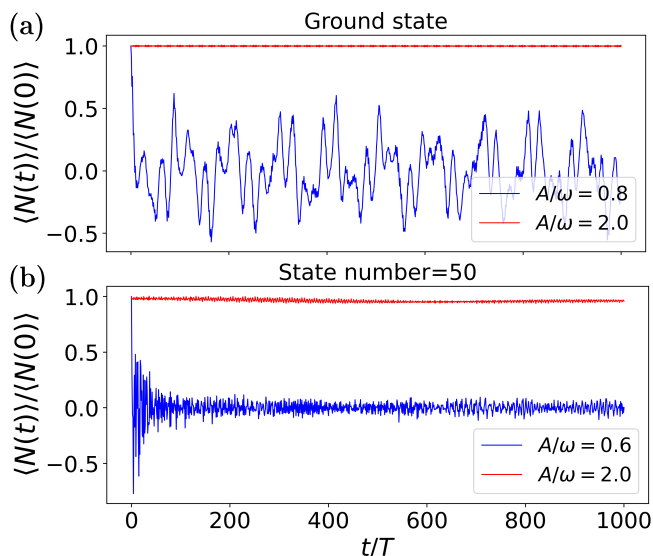


FIG. 14: Stroboscopic time evolution of normalized $\hat{N}(t)$ for different driving strengths for the square drive in Eq. 3a. The system size is $L = 6$, with an on-site Hilbert space dimension $\mathcal{H}_D = 4$. All other parameters are as in Fig. 2.

the robustness of freezing. Consider for simplicity starting with $\mathcal{H}_D = 2$ (i.e. equivalent to a spin-1/2 system). Recall that for the square-wave drive within the zeroth-order Magnus expansion, the non-integrable portion of the Hamiltonian is:

$$\frac{\omega E_J}{A\pi} \sin\left(\frac{\pi A}{\omega}\right) \sum_k \cos \hat{\varphi}_k - \frac{\omega E_J}{A\pi} \left(1 - \cos\left(\frac{\pi A}{\omega}\right)\right) \sum_k \sin \hat{\varphi}_k. \quad (\text{B.1})$$

The matrix elements in the basis states of interest are

$$\langle m_k | \cos \hat{\varphi}_k | n_k \rangle, \quad \langle m_k | \sin \hat{\varphi}_k | n_k \rangle, \quad (\text{B.2})$$

Performing a Taylor expansion of the $\cos \varphi$, $\sin \varphi$ terms in the transmon regime, we note that for the given \mathcal{H}_D , the former only contributes for $m = n$, while the latter contributes even when $m \neq n$.

If we recall the condition for freezing under the square-wave drive, we find that $A/\omega = 2\mathbb{Z}$, where both terms in Eq. B.1 vanish. However, in Fig. 12(a), we notice additional peaks not only at $A/\omega = 2\mathbb{Z}$ (even integer multiples) but also at odd integer values. For odd integer ratios of A/ω , the first term in Eq. B.1 goes to zero. Although the second term remains non-zero, its impact is less pronounced because it involves off-diagonal elements. In Fig. 12(b), we observe that as the ratio of amplitude to frequency increases, \mathcal{F} approaches 1 regardless of whether we are near or away from freezing. This is due to the effect of the nonintegrable part of the effective Hamiltonian being diminished quantitatively. It is noteworthy that a similar trend is evident in the plot of the Lyapunov exponent shown in Fig. 7(a). In Fig. 12(c) we show the initial state dependence on \mathcal{F} as a function of A/ω , which demonstrates that the robustness associated with the freezing peaks for the higher excited states (see Fig. 13) diminishes (Eq. B.1). We only observe the remaining freezing peaks for \mathcal{F} at the even integer ratios of A/ω . Finally, we have also studied the fate of freezing for the same square-wave drive protocol with local Hilbert-space dimension, $\mathcal{H}_D = 4$, as shown in Fig. 14.

-
- [1] J. M. Deutsch, “Quantum statistical mechanics in a closed system,” *Phys. Rev. A* **43**, 2046 (1991).
- [2] M. Srednicki, “Chaos and quantum thermalization,” *Phys. Rev. E* **50**, 888 (1994).
- [3] H. Tasaki, “From quantum dynamics to the canonical distribution: General picture and a rigorous example,” *Phys. Rev. Lett.* **80**, 1373 (1998).
- [4] M. Rigol, V. Dunjko, and M. Olshanii, “Thermalization and its mechanism for generic isolated quantum systems,” *Nature* **452**, 854 (2008).
- [5] D. M. Basko, I. L. Aleiner, and B. L. Altshuler, “Metal-insulator transition in a weakly interacting many-electron system with localized single-particle states,” *Annals of physics* **321**, 1126 (2006).
- [6] I. V. Gornyi, A. D. Mirlin, and D. G. Polyakov, “Interacting electrons in disordered wires: Anderson localization and low- t transport,” *Phys. Rev. Lett.* **95**, 206603 (2005).
- [7] R. Nandkishore and D. A. Huse, “Many-body localization and thermalization in quantum statistical mechanics,” *Annual Review of Condensed Matter Physics* **6**, 15 (2015), <http://dx.doi.org/10.1146/annurev-conmatphys-031214-014726>.
- [8] E. Altman and R. Vosk, “Universal dynamics and renormalization in many-body-localized systems,” *Annual Review of Condensed Matter Physics* **6**, 383 (2015), <http://dx.doi.org/10.1146/annurev-conmatphys-031214-014701>.
- [9] D. A. Abanin, E. Altman, I. Bloch, and M. Serbyn, “Colloquium: Many-body localization, thermalization, and entanglement,” *Rev. Mod. Phys.* **91**, 021001 (2019).
- [10] M. Serbyn, D. A. Abanin, and Z. Papić, “Quantum many-body scars and weak breaking of ergodicity,” *Nature Physics* **17**, 675 (2021).
- [11] A. Chandran, T. Iadecola, V. Khemani, and R. Moessner, “Quantum many-body scars: A quasiparticle perspective,” *Annual Review of Condensed Matter Physics* **14**, 443 (2023).
- [12] C. J. Turner, A. A. Michailidis, D. A. Abanin, M. Serbyn, and Z. Papić, “Weak ergodicity breaking from quantum many-body scars,” *Nature Physics* **14**, 745 (2018).
- [13] W. De Roeck and F. m. c. Huveneers, “Stability and instability towards delocalization in many-body localization systems,” *Phys. Rev. B* **95**, 155129 (2017).

- [14] S. Gopalakrishnan and D. A. Huse, “Instability of many-body localized systems as a phase transition in a non-standard thermodynamic limit,” *Phys. Rev. B* **99**, 134305 (2019).
- [15] J. vSuntajs, J. Bonvca, T. c. v. Prosen, and L. Vidmar, “Quantum chaos challenges many-body localization,” *Phys. Rev. E* **102**, 062144 (2020).
- [16] A. Morningstar, L. Colmenarez, V. Khemani, D. J. Luitz, and D. A. Huse, “Avalanches and many-body resonances in many-body localized systems,” *Phys. Rev. B* **105**, 174205 (2022).
- [17] D. Sels and A. Polkovnikov, “Thermalization of dilute impurities in one-dimensional spin chains,” *Phys. Rev. X* **13**, 011041 (2023).
- [18] K. Sacha and J. Zakrzewski, “Time crystals: a review,” *Reports on Progress in Physics* **81**, 016401 (2017).
- [19] D. V. Else, C. Monroe, C. Nayak, and N. Y. Yao, “Discrete time crystals,” *Annual Review of Condensed Matter Physics* **11**, 467 (2020).
- [20] M. P. Zaletel, M. Lukin, C. Monroe, C. Nayak, F. Wilczek, and N. Y. Yao, “Colloquium: Quantum and classical discrete time crystals,” *Rev. Mod. Phys.* **95**, 031001 (2023).
- [21] P. Ponte, Z. Papić, F. m. c. Huvneers, and D. A. Abanin, “Many-body localization in periodically driven systems,” *Phys. Rev. Lett.* **114**, 140401 (2015).
- [22] A. Lazarides, A. Das, and R. Moessner, “Equilibrium states of generic quantum systems subject to periodic driving,” *Phys. Rev. E* **90**, 012110 (2014).
- [23] L. D’Alessio and M. Rigol, “Long-time behavior of isolated periodically driven interacting lattice systems,” *Phys. Rev. X* **4**, 041048 (2014).
- [24] D. A. Abanin, W. De Roeck, W. W. Ho, and F. m. c. Huvneers, “Effective hamiltonians, prethermalization, and slow energy absorption in periodically driven many-body systems,” *Phys. Rev. B* **95**, 014112 (2017).
- [25] D. Abanin, W. De Roeck, W. W. Ho, and F. Huvneers, “A rigorous theory of many-body prethermalization for periodically driven and closed quantum systems,” *Communications in Mathematical Physics* **354**, 809 (2017).
- [26] T. Mori, “Floquet prethermalization in periodically driven classical spin systems,” *Phys. Rev. B* **98**, 104303 (2018).
- [27] N. O’Dea, F. Burnell, A. Chandran, and V. Khemani, “Prethermal stability of eigenstates under high frequency floquet driving,” *Phys. Rev. Lett.* **132**, 100401 (2024).
- [28] A. Das, “Exotic freezing of response in a quantum many-body system,” *Phys. Rev. B* **82**, 172402 (2010).
- [29] A. Haldar and A. Das, “Statistical mechanics of floquet quantum matter: exact and emergent conservation laws,” *Journal of Physics: Condensed Matter* **34**, 234001 (2022).
- [30] S. Bhattacharyya, A. Das, and S. Dasgupta, “Transverse ising chain under periodic instantaneous quenches: Dynamical many-body freezing and emergence of slow solitary oscillations,” *Phys. Rev. B* **86**, 054410 (2012).
- [31] S. S. Hegde, H. Katiyar, T. S. Mahesh, and A. Das, “Freezing a quantum magnet by repeated quantum interference: An experimental realization,” *Phys. Rev. B* **90**, 174407 (2014).
- [32] A. Haldar, R. Moessner, and A. Das, “Onset of floquet thermalization,” *Phys. Rev. B* **97**, 245122 (2018).
- [33] A. Haldar, D. Sen, R. Moessner, and A. Das, “Dynamical freezing and scar points in strongly driven floquet matter: Resonance vs emergent conservation laws,” *Phys. Rev. X* **11**, 021008 (2021).
- [34] S. Ghosh, I. Paul, and K. Sengupta, “Prethermal fragmentation in a periodically driven fermionic chain,” *Phys. Rev. Lett.* **130**, 120401 (2023).
- [35] B. Mukherjee, A. Sen, D. Sen, and K. Sengupta, “Dynamics of the vacuum state in a periodically driven rydberg chain,” *Phys. Rev. B* **102**, 075123 (2020).
- [36] B. Mukherjee, S. Nandy, A. Sen, D. Sen, and K. Sengupta, “Collapse and revival of quantum many-body scars via floquet engineering,” *Phys. Rev. B* **101**, 245107 (2020).
- [37] T. Banerjee and K. Sengupta, “Emergent conservation in the floquet dynamics of integrable non-hermitian models,” *Phys. Rev. B* **107**, 155117 (2023).
- [38] S. Ghosh, I. Paul, and K. Sengupta, “Signatures of fragmentation for periodically driven fermions,” (2024), [arXiv:2404.04328](https://arxiv.org/abs/2404.04328) [cond-mat.str-el].
- [39] A. Sen, D. Sen, and K. Sengupta, “Analytic approaches to periodically driven closed quantum systems: methods and applications,” *Journal of Physics: Condensed Matter* **33**, 443003 (2021).
- [40] S. Aditya and D. Sen, “Dynamical localization and slow thermalization in a class of disorder-free periodically driven one-dimensional interacting systems,” *SciPost Phys. Core* **6**, 083 (2023).
- [41] A. Das, Private communication.
- [42] H. Guo, R. Mukherjee, and D. Chowdhury, “Dynamical freezing in exactly solvable models of driven chaotic quantum dots,” (2024), [arXiv:2405.01627](https://arxiv.org/abs/2405.01627) [cond-mat.str-el].
- [43] A. Blais, A. L. Grimsmo, S. M. Girvin, and A. Wallraff, “Circuit quantum electrodynamics,” *Rev. Mod. Phys.* **93**, 025005 (2021).
- [44] J. Koch, T. M. Yu, J. Gambetta, A. A. Houck, D. I. Schuster, J. Majer, A. Blais, M. H. Devoret, S. M. Girvin, and R. J. Schoelkopf, “Charge-insensitive qubit design derived from the cooper pair box,” *Phys. Rev. A* **76**, 042319 (2007).
- [45] J. A. Schreier, A. A. Houck, J. Koch, D. I. Schuster, B. R. Johnson, J. M. Chow, J. M. Gambetta, J. Majer, L. Frunzio, M. H. Devoret, S. M. Girvin, and R. J. Schoelkopf, “Suppressing charge noise decoherence in superconducting charge qubits,” *Phys. Rev. B* **77**, 180502 (2008).
- [46] S.-D. Börner, C. Berke, D. P. DiVincenzo, S. Trebst, and A. Altland, “Classical chaos in quantum computers,” (2023), [arXiv:2304.14435](https://arxiv.org/abs/2304.14435) [quant-ph].
- [47] C. Berke, E. Varvelis, S. Trebst, A. Altland, and D. P. DiVincenzo, “Transmon platform for quantum computing challenged by chaotic fluctuations,” *Nature communications* **13**, 2495 (2022).
- [48] F. Yan, P. Krantz, Y. Sung, M. Kjaergaard, D. L. Campbell, T. P. Orlando, S. Gustavsson, and W. D. Oliver, “Tunable coupling scheme for implementing high-fidelity two-qubit gates,” *Phys. Rev. Appl.* **10**, 054062 (2018).
- [49] F. Arute, K. Arya, R. Babbush, D. Bacon, J. C. Bardin, R.arends, R. Biswas, S. Boixo, F. G. Brandao, D. A. Buell, *et al.*, “Quantum supremacy using a programmable superconducting processor,” *Nature* **574**, 505 (2019).
- [50] <https://quantumai.google>.
- [51] A. D. Córcoles, A. Kandala, A. Javadi-Abhari, D. T. McClure, A. W. Cross, K. Temme, P. D. Nation, M. Steffen, and J. M. Gambetta, “Challenges and opportunities of

- near-term quantum computing systems,” *Proceedings of the IEEE* **108**, 1338 (2020).
- [52] J. Preskill, “Quantum Computing in the NISQ era and beyond,” *Quantum* **2**, 79 (2018).
- [53] F. Nathan, L. O’Brien, K. Noh, M. H. Matheny, A. L. Grimsmo, L. Jiang, and G. Refael, “Self-correcting gkp qubit and gates in a driven-dissipative circuit,” (2024), [arXiv:2405.05671 \[cond-mat.mes-hall\]](https://arxiv.org/abs/2405.05671).
- [54] S. M. Girvin, “Circuit qed: superconducting qubits coupled to microwave photons,” (2014).
- [55] E. Bairey, G. Refael, and N. H. Lindner, “Driving induced many-body localization,” *Phys. Rev. B* **96**, 020201 (2017).
- [56] A. Eckardt, “Colloquium: Atomic quantum gases in periodically driven optical lattices,” *Rev. Mod. Phys.* **89**, 011004 (2017).
- [57] T. E. Roth, R. Ma, and W. C. Chew, “An introduction to the transmon qubit for electromagnetic engineers,” [arXiv preprint arXiv:2106.11352](https://arxiv.org/abs/2106.11352) (2021).
- [58] L. B. Nguyen, Y.-H. Lin, A. Somoroff, R. Mencia, N. Grabon, and V. E. Manucharyan, “High-coherence fluxonium qubit,” *Phys. Rev. X* **9**, 041041 (2019).
- [59] A. Gyenis, A. Di Paolo, J. Koch, A. Blais, A. A. Houck, and D. I. Schuster, “Moving beyond the transmon: Noise-protected superconducting quantum circuits,” *PRX Quantum* **2**, 030101 (2021).
- [60] <https://www.ibm.com/quantum/technology>.
- [61] J. Cohen, A. Petrescu, R. Shillito, and A. Blais, “Reminiscence of classical chaos in driven transmons,” *PRX Quantum* **4**, 020312 (2023).
- [62] S. H. Strogatz, *Nonlinear dynamics and chaos: with applications to physics, biology, chemistry, and engineering* (CRC press, 2018).
- [63] A. Eckardt and E. Anisimovas, “High-frequency approximation for periodically driven quantum systems from a floquet-space perspective,” *New journal of physics* **17**, 093039 (2015).
- [64] M. Bukov, L. D’Alessio, and A. Polkovnikov, “Universal high-frequency behavior of periodically driven systems: from dynamical stabilization to floquet engineering,” *Advances in Physics* **64**, 139 (2015).
- [65] X. Wang, S. Ghose, B. C. Sanders, and B. Hu, “Entanglement as a signature of quantum chaos,” *Phys. Rev. E* **70**, 016217 (2004).
- [66] L. Vidmar and M. Rigol, “Entanglement entropy of eigenstates of quantum chaotic hamiltonians,” *Phys. Rev. Lett.* **119**, 220603 (2017).
- [67] D. Hahn, P. A. McClarty, and D. J. Luitz, “Information dynamics in a model with Hilbert space fragmentation,” *SciPost Phys.* **11**, 074 (2021).
- [68] C. Tsitouras, “Runge–kutta pairs of order 5 (4) satisfying only the first column simplifying assumption,” *Computers & Mathematics with Applications* **62**, 770 (2011).
- [69] A. Vulpiani, F. Cecconi, and M. Cencini, *Chaos: from simple models to complex systems*, Vol. 17 (World Scientific, 2009).
- [70] G. Benettin, L. Galgani, A. Giorgilli, and J.-M. Strelcyn, “Lyapunov characteristic exponents for smooth dynamical systems and for hamiltonian systems; a method for computing all of them. part 1: Theory,” *Meccanica* **15**, 9 (1980).
- [71] G. Benettin, L. Galgani, A. Giorgilli, and J.-M. Strelcyn, “Lyapunov characteristic exponents for smooth dynamical systems and for hamiltonian systems: A method for computing all of them,” *Meccanica* **15**, 27 (1980).
- [72] G. Datseris, “Dynamicalsystems.jl: A julia software library for chaos and nonlinear dynamics,” *Journal of Open Source Software* **3**, 598 (2018).
- [73] S. E. Nigg, H. Paik, B. Vlastakis, G. Kirchmair, S. Shankar, L. Frunzio, M. H. Devoret, R. J. Schoelkopf, and S. M. Girvin, “Black-box superconducting circuit quantization,” *Phys. Rev. Lett.* **108**, 240502 (2012).
- [74] D. Sank, Z. Chen, M. Khezri, J. Kelly, R. Barends, B. Campbell, Y. Chen, B. Chiaro, A. Dunsworth, A. Fowler, E. Jeffrey, E. Lucero, A. Megrant, J. Mutus, M. Neeley, C. Neill, P. J. J. O’Malley, C. Quintana, P. Roushan, A. Vainsencher, T. White, J. Wenner, A. N. Korotkov, and J. M. Martinis, “Measurement-induced state transitions in a superconducting qubit: Beyond the rotating wave approximation,” *Phys. Rev. Lett.* **117**, 190503 (2016).
- [75] P. Weinberg and M. Bukov, “Quspin: a python package for dynamics and exact diagonalisation of quantum many body systems part i: spin chains,” *SciPost Physics* **2**, 003 (2017).
- [76] P. Weinberg and M. Bukov, “Quspin: a python package for dynamics and exact diagonalisation of quantum many body systems. part ii: bosons, fermions and higher spins,” *SciPost Physics* **7**, 020 (2019).